Journal of Molecular Graphics and Modelling 44 (2013) 91–103

Contents lists available at ScienceDirect

Journal of Molecular Graphics and Modelling

journal homepage: www.elsevier.com/locate/JMGM

Is the conformational flexibility of piperazine derivatives important to inhibit HIV-1 replication?

Cátia Teixeira[a,*], Nawal Serradji[a], Souad Amroune[a], Karen Storck[b], Christine Rogez-Kreuz[b], Pascal Clayette[b], Florent Barbault[a], François Maurel[a]

[a] Univ Paris Diderot, Sorbonne Paris Cité, ITODYS, UMR 7086, CNRS, 15 rue Jean Antoine de Baïf, F-75205 Paris, France
[b] Laboratoire de Neurovirologie, Bertin Pharma, CEA, F-92265 Fontenay aux Roses, France

ARTICLE INFO

Article history:
Accepted 5 May 2013
Available online 13 May 2013

Keywords:
HIV-1 gp120
BMS-378806
Piperazine derivatives
Conformational flexibility
Docking and molecular dynamics

ABSTRACT

The conserved binding site of HIV-1 gp120 envelope protein, an essential component in the viral entry process, provides an attractive antiviral target. The structural similarities between two piperazine derivatives: PMS-601, showing a dual activity for anti-PAF and anti-HIV activity, and BMS-378806, known to inhibit HIV-1 gp120, motivated us to merge important structural features of the two compounds. Novel piperazine derivatives were synthesized and evaluated *in vitro* concerning their ability to inhibit HIV-1 replication in *in vitro* infected lymphocytes. We described an approach that combines molecular docking, molecular dynamics, MM-PBSA calculations and conformational analysis to rationally predict piperazine derivatives binding mode with HIV-1 gp120. We also inquired about the conformational adaptability of the molecules, upon complex formation, and its importance to their respective inhibitory activity. The analysis suggested that the impact of the flexibility of these molecules revealed to be more important, in the context of drug design, than it has generally been assumed. These new insights at the atomic level might be useful to design inhibitors with improved antiviral activity.

1. Introduction

Attachment of the human immunodeficiency virus (HIV-1) to the cell surface is the first step of the virus cycle and it is mediated through the binding of the glycoprotein gp120 on the virion surface to a CD4 receptor on the host cell. Thus, the HIV-1 gp120 envelope protein is an essential component in the multi-tiered viral entry process and, despite the diversity in other gp120 domains, the conserved binding site that interacts with CD4 receptor provides an attractive antiviral target [1].

BMS-378806 (**1**, Fig. 1), a substituted piperazine compound bearing a 4-methoxy-7-azaindole group, protects target cells from HIV-1 infection at nanomolar levels [2]. Despite the controversy regarding the binding site on HIV-1 gp120 where this compound acts [3,4], more and more studies arisen to be consistent with the premise that BMS-378806 interacts with the CD4-binding pocket (called Phe43 cavity) of gp120 [5–7]. Thereby, by binding to gp120, BMS-378806 blocks the attachment of the virus to CD4 receptor. Given its good bioavailability, low protein binding and the promising potent antiviral activity, further development of other members of this class of compounds, piperazine derivatives, is certainly warranted and remains the subject of active research.

A decade ago, some of us found that PMS-601 (**2**, Fig. 1), a piperazine derivative substituted on nitrogen atoms with trimethoxyphenyl groups leading to "cache-oreilles" (ear-muff) electronic distribution, presents a dual activity with IC_{50} values of 8 and 11 μM for anti-platelet activation factor (anti-PAF) and anti-HIV activity, respectively. Additionally, the compound did not show cytotoxic events at 1000 μM in monocyte-derived macrophages [8]. We also established that: (i) the presence of a carbamate function was favourable to the antiviral activity of PMS-601 and (ii) the lipophilicity of the substituent on the piperazine cycle seemed to be less important for the anti-PAF activity than for the antiviral one. Although the mode of action responsible for the anti-HIV activity of PMS-601 is not clearly defined, it is a promising lead compound for the treatment of HIV infection and neuroAIDS, particularly, by combining its anti-PAF and anti-HIV-1 effects [9].

The structural similarities between PMS-601 and BMS-378806 (shortly named from now on BMS), motivated us to merge important structural features of the two compounds and engage in the development of novel piperazine derivatives (**8a**,**b**, Fig. 1) as potential antiretroviral agents. Hypothetically, molecules bearing key structural motif belonging to both PMS-601 and BMS would present an antiviral activity, more interesting than PMS-601, and using an

* Corresponding author. Current address: CICECO, Departamento de Química, Universidade de Aveiro, Campus Universitário de Santiago, P-3810-193 Aveiro, Portugal. Tel.: +351 234372571.
E-mail address: ca.teixeira@ua.pt (C. Teixeira).

1093-3263/$ – see front matter © 2013 Elsevier Inc. All rights reserved.
http://dx.doi.org/10.1016/j.jmgm.2013.05.003

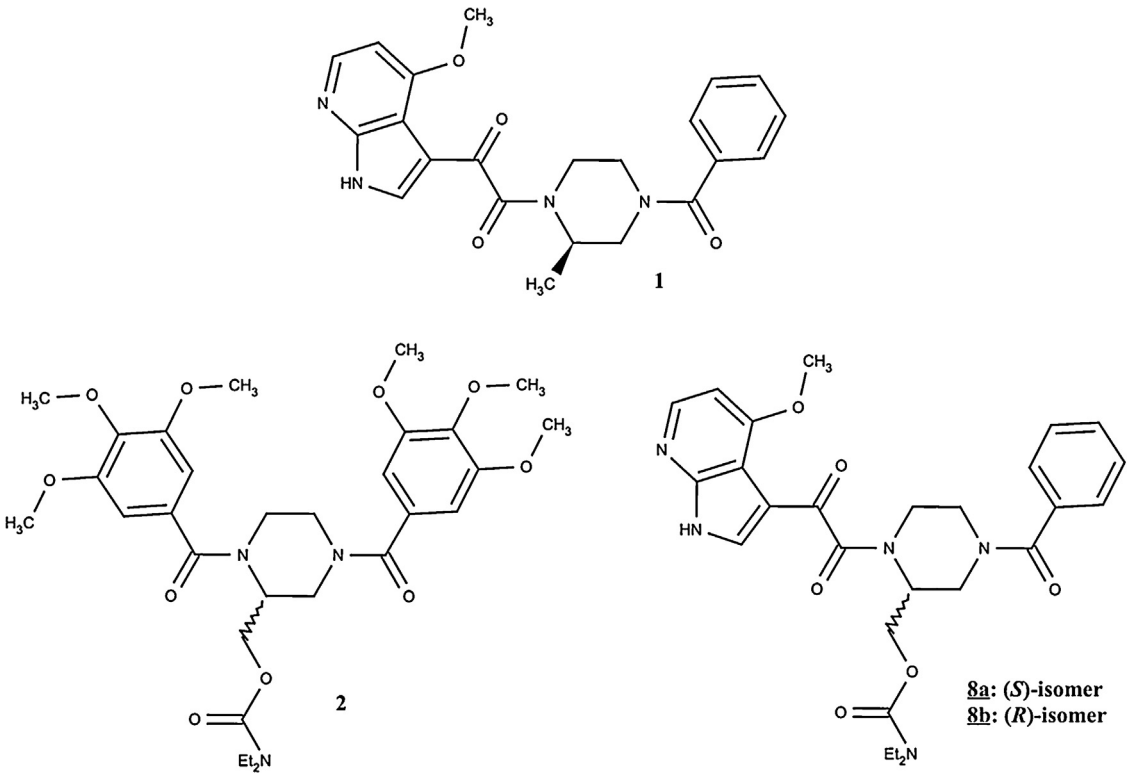

Fig. 1. Structures of BMS-378806 (**1**), PMS 601 (**2**) and synthesized compounds **8a** and **8b**.

identified mode of action, *i.e.*, the inhibition HIV-1 entry into cells by targeting the viral protein gp120. In this regard, novel piperazine derivatives were synthesized (Supp. Information, Scheme S1) and evaluated *in vitro* concerning their ability to inhibit HIV-1 replication in *in vitro* infected lymphocytes (Table 1).

None of the compounds showed significant anti-HIV-1 replication (Table 1). In order to understand the possible causes for this lack of activity and, consequently, design a second generation of compounds with an improved profile, molecular modelling studies were conducted. Specifically, we attempted to address the following questions: do the piperazine derivatives, **8a** and **8b**, bind to HIV-1 gp120 in a similar way that does BMS? How tightly the ligands bind to HIV-1 gp120? Which are the residues that establish stronger interactions with the ligands? How does the inhibitor conformational flexibility affect its affinity towards the target?

To answer to these questions, we used an approach combining molecular docking, molecular dynamics, MM-PBSA calculations and conformational analysis to rationally predict the binding mode of piperazine derivatives with HIV-1 gp120, inquire about the conformational adaptability of the molecules, upon complex formation, and its impact on their respective inhibitory activity. Since there is no crystal structure of a complex between gp120 and BMS, we first had to predict its binding mode by using molecular docking combined with molecular dynamics. It is important to refer that Kong and co-workers already carried out a previous study of rational prediction of the binding mode of BMS with HIV-1 gp120 wild-type (wt) [10]. In this study, they found that BMS inserts the azaindole ring deeply into the protein active site. Kong and co-workers put a lot of efforts into modelling protein's flexibility but they neglected the one of the ligand as their primary objective was to determine the precise gp120 binding site of BMS-378806. In fact, they assumed that BMS is rather rigid and the methoxy group on the azaindole was the only bond set as rotatable. However, it is well known that flexible molecules are deformed when binding to proteins, and thus, may bind as different conformers to them. The degree of deformation appears to depend somewhat upon the number of rotors in the ligand. Since BMS presents a high degree of flexibility it should be take into account during the molecular modelling studies. So, in order to validate our results for the predicted binding mode of BMS, we also performed the same molecular modelling procedure using the gp120 S375W as this mutation completely abates the inhibitory activity of BMS [7]. By running the same procedure with the mutant, we expected to observe the loss of the interactions between the residues of the binding site and BMS when compared to the results with the wild-type. Once we validated our procedure, we applied the same protocol for the novel piperazine derivatives, compounds **8a** and **8b**, which were also synthesized and their inhibition of HIV-1 binding determined.

To our knowledge this is the first study concerning the impact of the conformational adaptability of piperazine derivatives on their inhibition of HIV-1 gp120. The results obtained suggested that the impact of the flexibility of these molecules revealed to be more important, in the context of drug design, than it has generally been assumed. These new insights, at atomic level into the binding mode of piperazine derivatives and the impact of the flexibility of such molecules, might be useful to design improved inhibitors and make molecular modelling stand out as an important research tool for understanding experimental results.

Table 1
Anti-HIV-1-LAI effects and cytotoxicity of the tested compounds on activated PBMC *in vitro* infected by HIV-1-LAI.

Compound	ED_{50} (μM)	ED_{90} (μM)	CC_{50} (μM)	CC_{90} (μM)
AZT	0.03	0.12	–	–
BMS	<0.04	0.04	>125	>125
8a	>125	>125	>125	>125
8b	>125	>125	>125	>125

Results are expressed as ED_{50} and ED_{90}, concentration of drugs that decreases the HIV replication of 50% and 90%, respectively. CC_{50} and CC_{90}, concentration of drugs to reduce the viable cell number by 50% and 90%, respectively.

2. Experimental

Organic synthesis. Intermediate and target compounds were synthesized as described in Supporting Information.

Antiviral assay and cytotoxicity. One hundred thousand phytohaemagglutinin-P (PHA-P)-activated peripheral blood mononuclear cells (PBMC) treated by several concentrations of compound **8a** or **8b** were infected 30 min later with hundred 50% tissue culture infectious doses ($TCID_{50}$) of the HIV-1-LAI strain [11]. Previously, this virus was amplified *in vitro* on PHA-P-activated PBMC [12] and, viral stock was titrated using PHA-P-activated PBMC, and 50% $TCID_{50}$ calculated using Kärber's formula [13]. Compounds were maintained throughout the culture, and cell supernatants were collected at day 7 post-infection. Viral replication was then measured by quantifying reverse transcriptase (RT) activity in these cell culture supernatants (RetroSys, Innovagen). In parallel, cytotoxicity of the compounds was evaluated in uninfected PHA-P-activated PBMC by MTT assay on day 7. Experiments were performed in triplicate from one blood donor. Data analyses were performed using SoftMax® Pro 4.6 microcomputer software: percent of inhibition of RT activity or of cell viability were plotted *vs* concentration and fitted with quadratic curves; 50% and 90% effective doses (ED_{50} and ED_{90}) and cytotoxic doses (CC_{50} and CC_{90}) were calculated and compared between the tested compounds, AZT and BMS-378806 (Table 1).

2.1. Computational studies

Preparation of the protein and ligand structures. The starting coordinates of the protein were those of the X-ray crystal structure (PDB code: 1G9N) of HIV-1 gp120/CD4 receptor/17b antibody complex with a 2.9 Å resolution [14], from which the CD4 receptor and 17b fragment coordinates were removed. The protein gp120 presents variable loops with several mutations. Glu429 is one of these mutated residues and is located into the Phe43 cavity. With the module Biopolymer in Sybyl (version 7.3) molecular modelling program [15], we substituted Glu429 by a lysine, which is the corresponding residue in gp120 wt. Because the long distance between the Phe43 cavity and the others mutated residues, they were considered as gp120 wt residues. The protein was then minimized with AMBER9 [16] by 500 steps of steepest descent followed by 2000 steps of conjugate gradient to remove bad contacts using a generalized Born solvent model. The biomolecular force field ff03 was used [17]. The structure of gp120 S375W mutant was prepared following the same procedure as for gp120 wt. However, an additional residue, Ser375, was mutated to a tryptophan. The structure of compounds **1**, **8a** and **8b** were constructed and optimized using Sybyl 7.3 and Tripos foce field. Charges were assigned using the Gasteiger–Marsili method. Energy minimization was performed applying 20 simplex iterations followed by 1000 steps of Powell minimization until the gradient norm 0.05 kcal mol^{-1} was achieved. In all MD trajectories, a hydrogen bond was considered when the donor–acceptor distance was smaller than 3.5 Å and the donor–acceptor – H angle smaller than 60°. These weak criteria were chosen deliberately to count as much as possible hydrogen bonds even those which represent weak interactions.

Piperazine ring conformational search. The ligand, constructed with Sybyl, was prepared by using the antechamber module of AMBER. Atomic charges were derived with the AM1-BCC charge method [18]. The general AMBER force field, GAFF [19], was used. The molecules were minimized and a MD run of 10 ns was performed in vacuum at 300 K. The trajectory was saved every ps and the root mean square deviations (RMSD) fluctuations of the cycle atoms obtained over the 10 ns MD trajectory was calculated for the three ligands **1**, **8a** and **8b**.

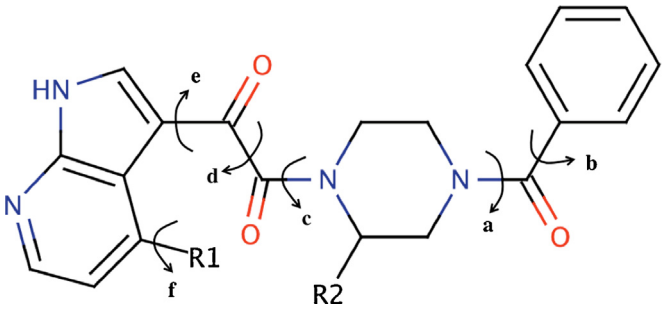

Fig. 2. Dihedral angles of the piperazine derivatives used (arrows) for the two-dimensional grid search.

Two-dimensional grid search. In order to gain information about the conformational flexibility and adaptability of the ligands, we performed a two-dimensional grid search with a semi-empirical method (AM1). The systematic search of the potential energy surfaces was carried out using the semi-empirical RHF-AM1 method [20], as implemented in the program AMPAC [21]. The dihedral angles a–b, c–d, d–e and e–f, represented in Fig. 2, were varied from 0° to 360° in intervals of 10° and an exhaustive RHF-AMl grid-search (36 × 36) was performed. While the two dihedrals were constrained to fixed increments, the remaining degrees of freedom were then relaxed and the geometry was optimized. The potential surface contour maps were drawn using Gnuplot [22].

Molecular docking. AutoDock 4.0 [23] was used in combination with the Lamarckian genetic algorithm (LGA) to treat the protein–inhibitor interactions and search for the suitable conformation. The protocol and parameters were set as described earlier [24]. During each docking experiment, 100 runs (the default value is 10) were carried out and at the end a cluster analysis was performed. Docking solutions with a ligand all-atom RMSD within 2 Å of each other were clustered together and ranked by the lowest docking energy. The selected binding modes selected for discussion were the ones belonging to the highest populated clusters with the lowest docking energy.

MD simulation. Molecular dynamics simulations of 8 complexes, HIV-1 gp120 wt with BMS (2 binding modes), compound **8a** (1 binding mode) and compound **8b** (3 binding modes) and HIV-1 gp120 S375W mutant with the two binding modes of BMS, were carried out using the AMBER9. His residues were set neutral with the default protonation state (HIE, with hydrogen on the epsilon nitrogen). The complex was soaked in a truncated octahedron box TIP3P [25,26] water molecules with a margin of 8 Å along each dimension. Four Cl^- ions were added to neutralize the system. The system was minimized stepwise: first minimizing only water/ions and then the entire system by 250 steps of steepest descent followed by 750 steps of conjugate gradient. The system was then heated from 0 to 300 K in 100 ps. A subsequent 5 ns production run was performed at a constant temperature of 300 K and a constant pressure of 1 atm with no constraint applied to either protein or the ligand. The Particle Mesh Ewald (PME) method [27] was applied to calculate long-range electrostatics interactions. All intermolecular interactions were treated with a cut-off distance of 12 Å. The SHAKE method [28] was applied to constrain all the covalent bonds involving hydrogen atoms thus the time interval was set to 2 fs. Coordinates were saved every 1 ps for a total of 5000 snapshots. The RMSD profiles for all the complexes of gp120 wt (some are available in supporting information) allowed us to verify that all the complexes achieved equilibration after 1 or 2 ns. Thus, for further analysis only the last 3 ns were considered. The residues in the 5 Å surrounding of the ligand were selected to calculate the interactions with the inhibitor and we will refer to those residues as binding pocket. We then carried out the MD simulations for each

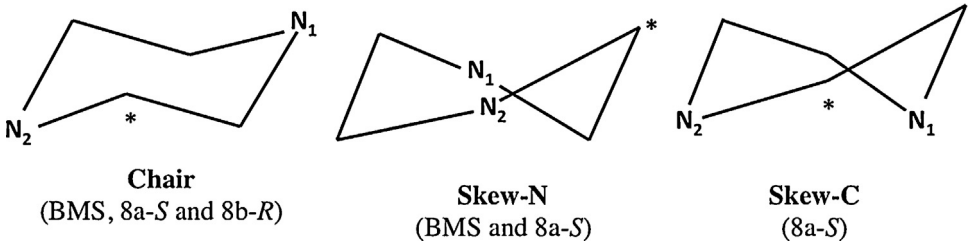

Fig. 3. Different piperazine conformers extracted for BMS and compounds **8a** and **8b**. The asterisk indicates the chiral carbon of the piperazine cycle.

ligand free in solution with the same parameters and procedure as the MD simulations of the complexes.

MM-PBSA calculation. The binding free energies were calculated using the MM-PBSA method [29]. A total number of 600 snapshots were taken from the last 3 ns of the MD trajectories with an interval of 5 ps. The unbound inhibitors and protein were also taken from the respective complexes trajectory. The explicit water molecules and ions were removed from the snapshots. The binding free energy, ΔG_{bind}, was estimated from computational analysis of a single simulation of the ligand–protein complexes and includes computed components corresponding gas-phase ligand–protein interactions (ΔE_{MM}), conformational entropy ($T\Delta S$) and solvation contributions (ΔG_{solv}). The gas-phase interaction energy between the protein and the ligand, ΔE_{MM}, is the sum of electrostatic and van der Waals interaction energies. The solvation free energy, ΔG_{solv} is the sum of polar (ΔG_{PB}) and nonpolar (ΔG_{np}) parts. The ΔG_{PB} term was calculated by the finite-difference solution of the Poisson–Boltzmann equation [30]. The dielectric constant was set to 1 for the interior solute and 80 for the surrounding solvent. The nonpolar contribution was determined on the basis of solvent-accessible surface area (SASA) using MOLSURF program [31], which is directly related to solvent accessible surface area: $\Delta G_{np} = 0.00542$ (SASA) + 0.92 [32]. The entropy component, $T\Delta S$, in Eq. (1) was estimated by normal mode computations, from 60 snapshots taken at 50 ps intervals from the last 3 ns of MD trajectory, calculated with the AMBER 9 NMODE program [33]. As mentioned, we have used a single molecular dynamics protocol and as a consequence, the contribution of internal energy to the binding free energy is equal to zero.

Decomposition of free energy on a per-residue basis. The per-atom contributions can be summed over atom groups such as residues, backbone and side-chains, to obtain their contributions to the total binding free energy [34]. Thus, contributions due to interactions between the ligands and the binding pocket residues were calculated at the atomic level using the MM-GBSA module [35] in AMBER 9.

3. Results and discussion

3.1. Antiviral assays

Synthesis description, detailed spectroscopic and analytical data on test compounds **8a**, **8b** and respective intermediates are available in supporting information. The anti-HIV activities of the synthesized compounds were assayed according to previously described methods [11,36] using PHA-P-activated PBMC *in vitro* infected with HIV-1-LAI [36]. Results are presented in Table 1.

As described in the literature, **BMS** greatly decreases HIV-1 replication in PBMCs without cytotoxicity ($CC_{50} > 125$ μM). In contrast, the introduction of the carbamate function of **PMS 601** led to inactivity in both compound **8a** and its isomer, compound **8b**.

Conformational analysis of the piperazine ring. We carried out molecular dynamics simulations for the small molecules and extracted all the possible cycle conformers to be used as input in the molecular docking studies, which normally do not allow the modelling of the cycle's flexibility. From 10 ns molecular dynamics (MD) we determined the predominant conformations that the piperazine ring could adopt. Fig. 3 resumes the different cycle conformers found for each compound and the RMSD graphs for the 3 compounds are available in supporting information (Figure S1).

We obtained distinct conformations for BMS and compounds **8a** and **8b**: two (chair and skew-N, Fig. 3), three (chair, skew-N and skew-C, Fig. 3) and one (chair, Fig. 3), respectively. This different result for the two chiral molecules, **8a** and **8b**, suggests that the carbamate group directly affects the conformation of the piperazine ring by steric effect.

3.2. Molecular docking analysis of BMS with HIV-1 gp120 wt and S375W mutant

For both, chair and skew-N cycle conformations, the same two binding modes were observed. In both cases, the ligand either inserts the phenyl moiety (phenyl binding mode) or the azaindole group (azaindole binding mode) of BMS into the active site of the protein. The same binding modes of the two cycle conformers were very similar as it can be seen in Fig. 4. The azaindole moieties in the azaindole binding modes are completely superposed (Fig. 4 – left) for both cycle conformers only diverging slightly for the rest of the molecule due to the different cycle conformation. Phenyl binding mode (Fig. 4 – right) does not present the same degree of superposition between chair and skew-N conformations as observed for the azaindole orientation; even so, we assumed they are very similar.

From these results it can be concluded that (i) the piperazine conformation does not seem to significantly influence the binding mode of BMS with gp120, (ii) the phenyl and azaindole binding modes obtained for BMS with the chair conformation present lowest docking energies (−12.4 and −12.5 kcal mol^{-1}, respectively) than their corresponding binding modes for BMS with the skew-N conformation (−12.1 and −11.5 kcal mol^{-1}, respectively) and (iii) the chair conformation is the predominant conformation during the last 5 ns of BMS MD (*cf.* conformational analysis of piperazine ring). For further studies, we considered only the two binding modes issued from the chair conformation.

Table 2
H bonds formed between wild-type gp120 and phenyl and azaindole orientations of BMS.

	Donor	Acceptor	Duration (% of the total simulation time considered)	Mean distance (Å)	Mean angle (°)
BMS phenyl	N_{ar} (BMS)	H—N (Gly431)	98	3.0	22
BMS azaindole	O (Ser256)	H—N (BMS)	93	3.0	27

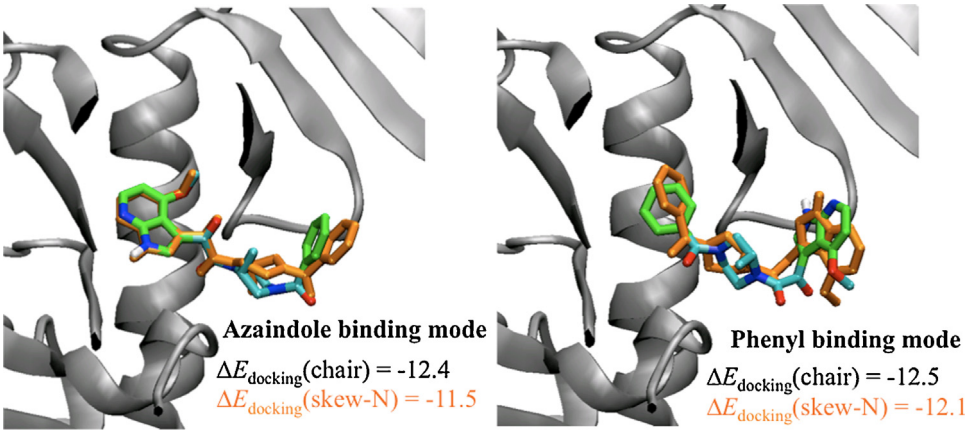

Fig. 4. Azaindole (left) and phenyl orientations (right) of docked BMS with gp120 wt, obtained for the molecule with the chair (colours) and skew-N (orange) piperazine conformers. The values of docking energy (kcal mol^{-1}) for the different docked conformations of BMS are also indicated. (For interpretation of the references to colour in this figure legend, the reader is referred to the web version of the article.)

Since the ring conformation of BMS did not seem to influence its binding conformation, we only used the structure of BMS with the piperazine presenting the chair conformation as starting structure for the molecular docking study with gp120 S375W. We obtained the same two distinct binding modes, azaindole and phenyl (Supp. Information, Figure S2). However, when comparing their docking energies, −9.0 and −8.8 kcal mol^{-1} for azaindole and phenyl, respectively, with the ones obtained for gp120 wt, −12.4 and −12.5 kcal mol^{-1}, respectively, we verified a more positive value in both cases. This was not surprising as BMS loses its biological activity when interacting with S375W-gp120 [7]. But again, we obtained very similar values of docking energy for two very different binding modes, which did not permitted us to discriminate one of them. Thus, both complexes with gp120 S375W were selected for further molecular dynamics studies.

3.3. Molecular docking analysis of compounds **8a** and **8b** with HIV-1 gp120 wt

The docking results of **8a** with gp120 wt showed that, regardless the conformation of the cycle (chair, skew-N and skew-C), **8a** always adopted a phenyl orientation, *i.e.*, placing the phenyl moiety into the active site of the protein. These three binding modes, provided with supporting information (Figure S3), were all quite similar in the sense that the carbamate group and azaindole are always located in the same environment of the protein. The phenyl moiety is situated at the entrance of the binding site while the carbamate group is orientated to accommodate between the entrance of the cavity and the labile bridging sheet of the protein (residues 119–129 and 194–203), and the azaindole moiety is orientated to interact with a slight protuberance of gp120 opposite to the labile bridging sheet. Since all the phenyl orientations were structurally similar, the one presenting the lowest energy of docking (−14.1 kcal mol^{-1}), which corresponds to the structure with the skew-N piperazine ring conformation (Fig. 5A), was selected for further analysis.

Although compound **8b** presented only one predominant piperazine conformation (chair), we obtained three different probable binding modes with similar docking energies (Fig. 5). One of the **8b** binding modes (named cap – Fig. 5B) placed the piperazine ring parallel to the entry of the cavity, resembling a "bottle stopper". The second one (named azaindole – Fig. 5C) inserted the azaindole ring at the entrance of the gp120 active site, which is filled by the phenyl moiety in the third binding mode (named phenyl – Fig. 5D). Also, all of the docking poses presented more positive energies of docking than **8a**, suggesting that the enantiomer (*S*) establish more favourable interactions with the binding site. Since energetic criterion did not allow us to discriminate between the three binding modes obtained for **8b**, all were selected for further molecular dynamic studies.

3.4. Molecular dynamics of complexes of gp120 wt with BMS azaindole and phenyl binding modes

Monitoring of kinetic, potential, and overall energies along the trajectory, as well as the density, pressure, and temperature, demonstrated the stability of the gp120/ligands complexes. For all systems, RMSD curves of selected residues were produced, along the trajectories, to observe molecular movements and fluctuations.

From the tracking of H bonds (Table 2) along the analysed trajectories, a main interaction (up to 70% of time) is observed between NH of the azaindole moiety and the carbonyl backbone of Ser256 for the complex gp120 wt with the azaindole binding mode. Regarding the complex of gp120 with BMS phenyl binding mode, the only observed main H bond taken place between N_{ar} of the six-membered ring of the azaindole moiety and the backbone NH of Gly431.

Table 3 shows the interactions energies, between the two possible orientations of BMS with the main binding pocket residues, decomposed into apolar ($\Delta E_{vdw} + \Delta G_{(GB)np}$) and polar contributions ($\Delta E_{ele}\Delta G_{(GB)p}$). The azaindole orientation presents slightly higher values for both apolar and polar contributions than the phenyl orientation, being the larger difference observed for the apolar interactions, which were the main favourable contribution to the binding of both ligands.

Fig. 6 shows the residues that mainly contribute to the binding affinity ($\Delta G_{gas+solv} < -2.0$ kcal mol^{-1}) of phenyl (Fig. 6A) and azaindole (Fig. 6B) binding modes. In blue are represented the amino acids that predominantly interact with the azaindole orientation, in red the residues that mostly form interactions with the phenyl orientation and in yellow the amino acids that present major interactions with both orientations.

The two binding modes establish interactions with common residues but if we observe the residues that interact only (or predominantly) with one of the two orientations, we can infer some interesting features:

(i) The residues that interact with both orientations (Thr257, Glu370, Asn425, Trp427 and Met475) are mainly located at the entrance of the Phe43 cavity.

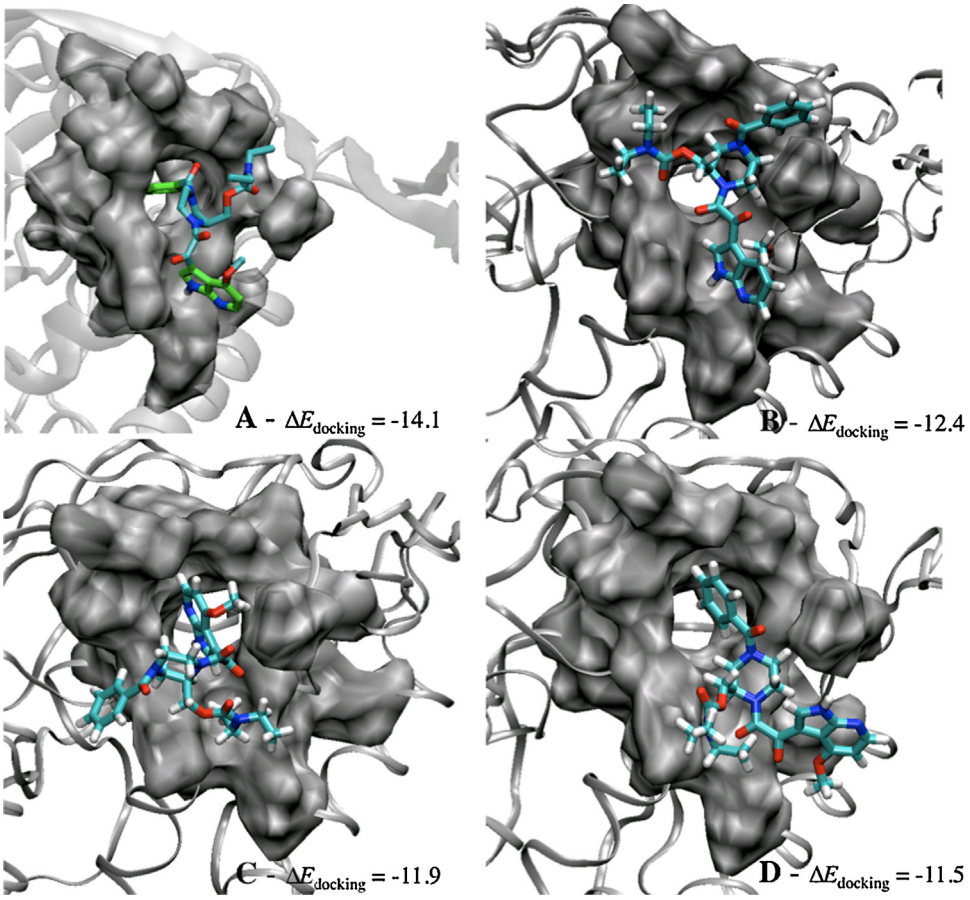

Fig. 5. Selected binding modes of compounds **8a** (A) and **8b** (B–D) with HIV-1 gp120 wt for molecular dynamics studies. (A) Represents the phenyl binding mode with the skew-N cycle conformation for compound **8a** while (B), (C) and (D) represents the **8b** binding modes cap, azaindole and phenyl, respectively, and all with the chair cycle conformation.

(ii) The azaindole orientation formed main interactions with amino acids that are situated deeper into the pocket (Phe382, Val255 and Ser256) as a consequence of being inserted more deeply into the cavity than the phenyl binding mode.
(iii) Unlike what it was observed in (ii), the residues that predominantly interacted with the phenyl orientation are all situated prior to the entrance of the Phe43 cavity.
(iv) W112A, T257R and F382L gp120 mutants completely prevent the binding of BMS [7]. The complex of gp120 with azaindole binding mode is consistent with this experimental data as, unlike for phenyl binding mode, all three residues form favourable interactions with the ligand, which suggest that the azaindole orientation may be the preferred binding mode. This hypothesis was further supported by the estimation of the free energy of binding of the two complexes.

Table 4 reports the calculated binding free energies (ΔG_{bind}) for the two orientations of BMS with gp120 wt. The azaindole binding mode presented the most favourable binding free energy, −39.0 kcal mol^{-1}, about 3 kcal mol^{-1} more negative than the phenyl orientation, −35.8 kcal mol^{-1}. For the two binding modes, the electrostatic energies were not very different in

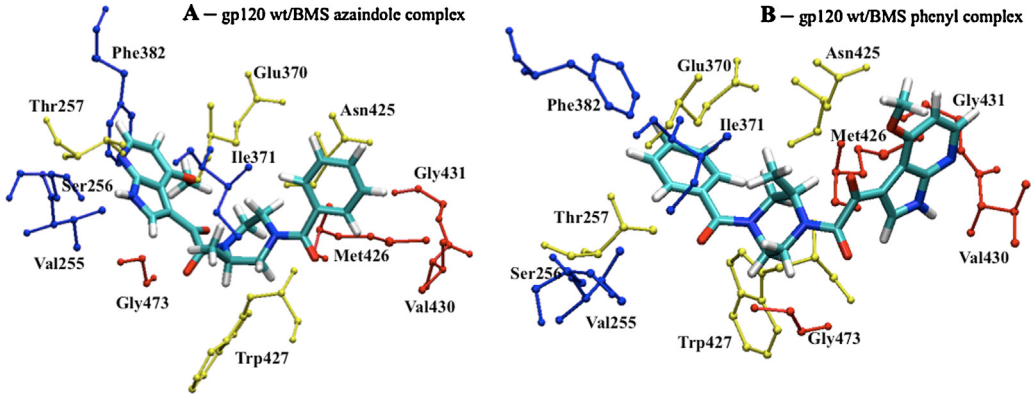

Fig. 6. Azaindole (A) and phenyl (B) orientations of BMS complexed with gp120 wt. The binding pocket residues that create specific interactions with the azaindole and phenyl orientations are represented in red and blue, respectively. In yellow are displayed the residues of the protein that form main contacts with both binding modes.

Table 3
Decomposition of ($\Delta G_{gas+solv}$) on a pairwise-residue basis into apolar ($\Delta E_{vdw} + \Delta G_{(GB)np}$) and polar contributions ($\Delta E_{ele}\Delta G_{(GB)p}$), for the complexes of wt-gp120 with phenyl and azaindole orientations of BMS. Values in bold represent significant interactions ($\Delta G_{gas+solv} < -2.0$ kcal mol^{-1}) to the binding free energy.

Residue number[a]	BMS_phenyl			BMS_azaindole		
	Apol[b]	Pol[c]	Total	Apol	Pol	Total
Val255	−1.1	−0.3	−1.4	**−2.6**	**−0.3**	**−2.9**
Ser256	−0.9	0.2	−0.7	**−1.6**	**−2.5**	**−4.1**
Thr257	**−1.9**	**0.0**	**−1.9**	**−1.5**	**−0.7**	**−2.3**
Glu370	**−3.6**	**0.1**	**−3.4**	**−5.5**	**0.0**	**−5.4**
Ile371	−1.2	0.0	−1.2	**−4.3**	**−0.2**	**−4.5**
Phe382	−0.7	0.1	−0.7	**−2.3**	**−0.1**	**−2.4**
Asn425	**−4.8**	**−0.5**	**−5.3**	**−3.9**	**−0.2**	**−4.1**
Met426	**−2.1**	**−1.4**	**−3.4**	−1.5	0.0	−1.5
Trp427	**−3.7**	**0.0**	**−3.7**	**−4.6**	**0.2**	**−4.4**
Val430	**−2.2**	**−0.8**	**−3.0**	−0.3	0.0	−0.3
Gly431	**−1.1**	**−1.0**	**−2.1**	−0.2	0.0	−0.1
Gly473	**−2.1**	**0.3**	**−1.9**	−0.8	0.0	−0.8
Met475	**−1.7**	**−0.1**	**−1.8**	**−2.4**	**−0.5**	**−2.9**
Total	−27.1	−3.4	−30.5	−31.5	−4.3	−35.7

All energies are in kcal mol^{-1}.
[a] The residue number is according to the HIV-1 gp160 sequence.
[b] Apol = $\Delta E_{vdw} + \Delta G_{(GB)np}$.
[c] Pol = $\Delta E_{ele} + \Delta G_{(GB)p}$.

contrary to the apolar/hydrophobic energies ($\Delta E_{vdw} + \Delta G_{np}$), −82.1 and −91.4 kcal mol^{-1} for phenyl and azaindole binding modes, respectively. These MD results suggest that BMS interacts more strongly with the Phe43 cavity of gp120 through the azaindole rather than the phenyl binding mode.

In order to confirm and validate our previous findings, we performed MD simulations of the complexes of these two orientations with gp120 S375W. This protein is a gp120 mutant that completely negates the binding to BMS and then, we expect that the preferred binding mode with gp120 wt will not act as a stable system during the MD trajectory. This way, the system that will show more instability will correspond, *a priori*, to the complex between the mutant and the preferred binding mode.

3.5. Molecular dynamics of complexes of gp120 S375W with BMS azaindole and phenyl binding modes

Looking at the RMSD profile of the complexes of gp120 S375W with BMS azaindole (Supp. Information, Figure S6), we observed important conformational changes the ligand and binding pocket residues between 2.5 and 3 ns and a slow increase in its RMSD until the end of the trajectory. Concerning the system of gp120 S375W with phenyl orientation, we did not observe any stability either. The RMSD values of the binding pocket residues increased progressively along the time simulation while for the ligand we only observed an increase in its RMSD value for the last 200 ps of the simulation. Despite the complex of the mutant and phenyl orientation never reached stability, it does not present any abrupt conformational change as we verified for the azaindole binding mode.

Fig. 7A shows the position of the azaindole binding mode with gp120 S375W at different times of the trajectory. The ligand is represented in colours and black at 100, and 5000 ps, respectively. At 100 ps, the azaindole ring is placed at the entrance of the cavity and the phenyl moiety is situated at the right side of the entrance pointing to the arm of the protein. Along the trajectory, we observed that the ligand is progressively "kicked out" until it is completely out of the binding pocket, establishing no interactions with the gp120 S375W, as we noticed at 5000 ps.

A completely different behaviour is obtained for the complex of gp120 S375W with the phenyl orientation (Fig. 7B). Indeed, we observed that the ligand evolved in order to bind tightly to the protein. At 100 ps, the phenyl moiety is placed perpendicularly into the Phe43 cavity and fits well into it. In addition, the azaindole group forms three H bonds with the residues in its surrounding. One H bonds is detected between the NH group of azaindole group and the Asp474 side chain, and the other two involve N_{ar} atom of the six-membered ring with NH_2 group of Arg476 and NH group of His105. At 5000 ps, we observed a conformational change of the ligand, corresponding to the increase in RMSD value for the last 200 ps of the trajectory, and during which the phenyl moiety is placed parallel to the cavity and, consequently, the entire molecule get closer to it.

We believe that, after this conformational change of the phenyl orientation, the system would have reached stability. In order to get more information about the interactions that would have established with the protein after the complex has got stability, we should have proceeded with the simulation. However, the main objective was to confirm and validate the results obtained with the MD simulations of the complexes with gp120 wt. In this regard, the results presented above strongly support that the azaindole orientation id the predominant binding mode to HIV-1 gp120 wt.

3.6. Conformational adaptability of BMS

Flexible molecules may change their conformation when binding to a protein and thus present several different possible binding modes. Actually, it has been observed that in the majority of cases the binding conformation of a flexible ligand does not correspond to the global energy minimum of the same ligand in its free state, and in many cases it does not even correspond to a local minimum [37,38]. Thus, the conformational energy required for that ligand to adopt its binding conformation may significantly affect the affinity of the ligand towards its target. In order to inquire about the conformational flexibility and adaptability of the ligands, a two-dimensional grid search with a semi-empirical method (AM1) was performed.

Fig. 8 shows the contours of potential energies (kcal mol^{-1}) for different values of dihedrals pair c–d, where each colour represents a relative energy value above the global minimum. We verified that the dihedrals pairs a–b, d–e and e–f (*cf.* Fig. 2) can be varied

Table 4
MM-PBSA interactions energies for the complexes of gp120 wt with phenyl and azaindole binding modes of BMS.

Contribution	BMS_phenyl		BMS_azaindole	
	Mean (kcal mol^{-1})	STD (kcal mol^{-1})	Mean (kcal mol^{-1})	STD (kcal mol^{-1})
ΔE_{ele}	−7.0	3.9	−15.4	3.3
ΔE_{vdw}	−45.8	2.6	−53.0	2.6
ΔE_{gas}	−52.8	4.2	−68.5	3.7
ΔG_{np} (solvation, non-polar)	−36.3	0.8	−38.4	1.0
ΔG_{p} (solvation, polar)	32.1	3.6	43.2	3.3
$\Delta E_{gas} + \Delta G_{solv}$	−57.0	3.6	−63.6	3.5
$-T\Delta S_{gas}$	21.2	7.9	24.6	11.3
ΔG_{bind}	−35.8	8.7	−39.0	11.8

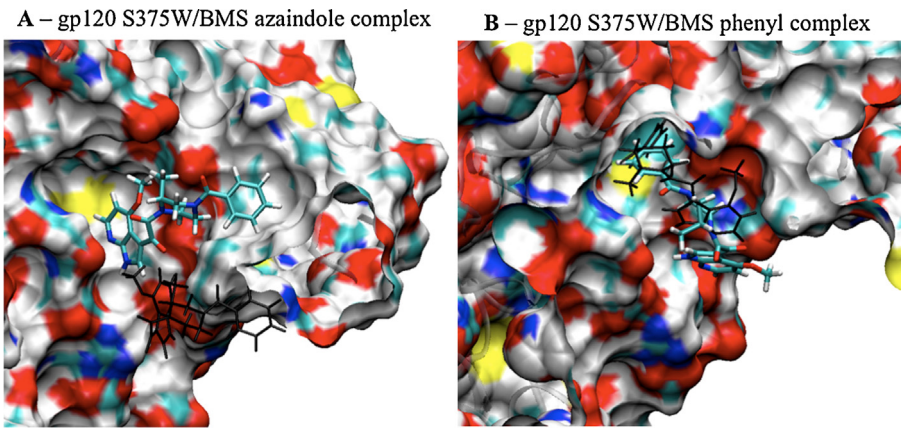

Fig. 7. Representation of the surface of gp120 S375W with the azaindole (A) and phenyl (B) binding modes at 100 (colours) and 5000 (black) ps of the MD trajectory.

without encountering significant energy barriers, which was not the case for dihedral pair c–d. We superimposed the values of the calculated dihedrals of BMS along the MD trajectory of the ligand free in solution (blue) and for azaindole (orange) and phenyl (green) orientations bound to gp120 wt.

We observed that the conformational change that BMS undergoes, to bind to gp120 wt through the azaindole orientation, demands very low energy penalty (about 2 kcal mol^{-1}) compared to the one observed for the phenyl orientation (10 kcal mol^{-1}). This conformational analysis revealed that the azaindole conformation is more accessible to protein binding than the phenyl orientation.

3.7. BMS – azaindole vs. phenyl binding mode

Should we completely discard the phenyl orientation as a possible binding mode to HIV-1 gp120? Based on our results, we do not believe so. We found evidences that point the azaindole orientation as the preferred binding mode, which does not mean that the phenyl orientation is an invalid binding mode. Indeed, the same way the results showed that azaindole is the predominant orientation that interacts with gp120, they also sustained the phenyl mode as another conformation through which BMS can bind to the protein. Thus, we here put forward the theory that BMS can bind to HIV-1 gp120 with two conformationally distinct binding modes but only one is "bioactive". We should remember that BMS inhibits the protein by binding to the Phe43 cavity, which corresponds to a specific area within the molecular interface between CD4 and gp120. Consequently, BMS is a small molecule that directly competes with CD4 receptor for gp120 binding. Thus, we assume that the ligand presents two possible binding modes but only the "bioactive" one has the ability to compete with CD4 for gp120 binding.

A recent study showed that small-molecule ligands with strategic degrees of conformational freedom can wiggle and jiggle to adapt to variant compositions of a binding pocket, thereby overcoming resistance [39]. BMS has those strategic degrees of conformational freedom, however it misses the part of the accessibility of the different conformers to protein binding. Concerning the overcoming resistance of BMS, we think that the phenyl

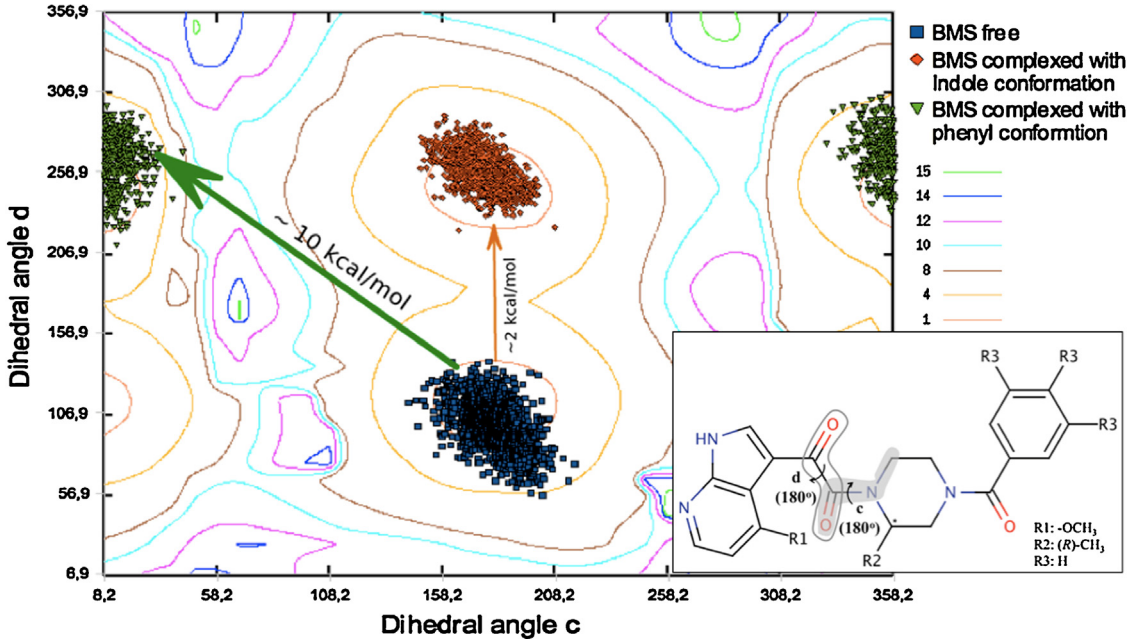

Fig. 8. Contours of potential energy for the dihedral pair c–d of BMS. The value of the dihedrals angles c–d for the free state, the azaindole and phenyl orientation of BMS complexed with wt-gp120, are represented in blue, orange and green, respectively. The arrows show the conformational change that the free ligand needs to undergo to adopt the azaindole (orange) and phenyl binding mode (green). (For interpretation of the references to colour in this figure legend, the reader is referred to the web version of the article.)

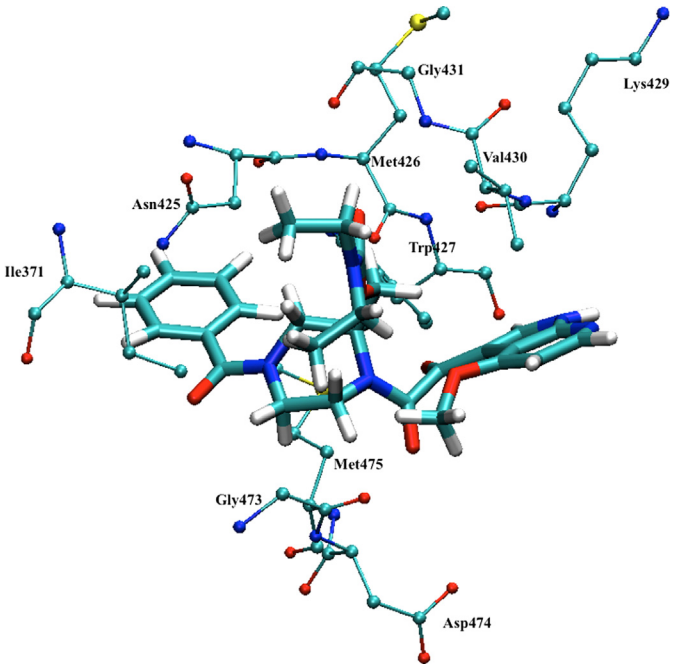

Fig. 9. Average structure of the complex of gp120 wt with compound **8a** and the respective binding pocket residues.

orientation would be more attractive than the azaindole one. Indeed, we observed that for the S375W gp120 mutant, theoretically and in addition of presenting binding affinity to gp120 wt, phenyl orientation is able to overcome resistance contrary to azaindole orientation, which was ejected from the binding site of S375W gp120 and only presented affinity to the wild-type. Therefore, it would be of interest to turn the phenyl conformation more competitive by modifying the structure of ligand so the conformational change, between BMS free in solution and its conformation upon binding, presents a lower penalty of energy, and thereby escapes the effects of drug-resistance mutations.

3.8. Molecular dynamics of complexes of gp120 wt with compound *8a* binding mode

Fig. 9 represents the average structure of the complex between gp120 wt and compound **8a**. From the hydrogen bonding patterns analysis, we found that two main H bonds (Table 5) were established between compound **8a** and the binding pocket residues: the backbone NH of Met475 with the carbonyl of α-ketoamide moiety, in the vicinity of the piperazine ring, and the backbone NH of Gly431 with the carbonyl of the carbamate group. The residues, Met475 and Gly431, are located at the entrance of the cavity and the H bonds formed with compound **8a** contribute to keep the phenyl moiety inside the cavity while the rest of the molecule is involved in hydrophobic interactions with residues outside.

The interaction energies between compound **8a** and the amino acids of the protein are shown in Table 6. Globally, we observed that the binding affinity of compound **8a** is mainly due to apolar/hydrophobic terms rather than polar interactions, which was also observed for the azaindole conformation of BMS. Moreover, when compared to BMS, we noticed that molecule **8a** presented more affinity (more negative values of interaction energies) with a higher number of residues. The strongest interactions were observed with Val430 and Met475.

Table 7 reports the calculated binding free energies (ΔG_{bind}) between compound **8a** and gp120 wt. Comparing to BMS, a most favourable binding free energy was obtained for compound **8a** (-44.7 kcal mol^{-1}) about 6 kcal mol^{-1} more negative than for the azaindole conformation of BMS.

3.9. Molecular dynamics of complexes of gp120 wt with binding modes of compound *8b*

Fig. 10 represents the RMSD profiles (Fig. 10A–C) and the average structures (Fig. 10D–F) issued from the MD simulation. Regarding the movements made along the simulation, we noticed that the different systems presented distinct behaviours: (i) the complex with the cap orientation (Fig. 10A) presents a sharp increase in RMSD values, for both binding pocket residues and ligand, at the beginning of the trajectory stabilizing just after; (ii) the complex with the azaindole binding mode (Fig. 10B) exhibited the lowest stability of the three systems; (iii) for the complex with the phenyl orientation (Fig. 10C), both binding pocket amino acids and inhibitor presented a good stability with RMSD values that barely exceeded 1.5 Å. The phenyl orientation presented small variation of RMSD, indicating that no large conformational change was made to reach equilibration. Concerning the hydrogen bonds established between the different binding poses of compound **8b** and gp120 wt, we observed only one main contact for both cap (azaindole nitrogen with His105 NH backbone) and phenyl (carbamate carbonyl with Arg476 side chain) orientations.

Table 6 reports the interaction energies between compound **8b** and the binding site residues. As for BMS and compound **8a**, we observed that the binding affinities of the three orientations with the binding-site residues are mainly achieved by apolar/hydrophobic terms. The residues interacting most with the cap orientation of compound **8b** are mainly situated at the entrance of the Phe43 cavity forming stable interactions with the ligand. For the phenyl binding mode, the *quasi* totality of key residues establishing favourable contacts with it is also highlighted for the cap binding mode, indicating a high similarity, in terms of contacts with the protein, between these two binding modes. Regarding the azaindole binding mode, both apolar an apolar contacts were found to be weaker than for the other two binding modes.

The different binding energy components were calculated between ligand and protein during the simulations, and the results are shown in Table 7. The binding free energy of cap conformation is the most negative of the three possible binding modes, with a value of -34 kcal mol^{-1}, while the phenyl orientation registered a binding free energy of -31.9 kcal mol^{-1}. The favourable contributions to the binding affinity predominantly result from the nonpolar terms ($\Delta E_{vdw} + \Delta G_{np}$). Comparing the ΔG_{bind} value of azaindole binding mode, -25.7 kcal mol^{-1}, with the other two binding modes reveals a large difference in its binding affinity. Considering that compound **8b** presents the same chirality (*R*) as BMS and that the only structural difference is the replacement of the piperazine substituent methyl by a carbamate group, these results suggest that a bulkier group at R2 position hinder the azaindole moiety to enter deeper within the binding pocket. As a consequence, interactions with residues located deeper in the active site are lost as we observed for azaindole orientation of compound **8b**, for example Ser256 and Trp427, when compared to the azaindole binding mode of BMS. Additionally, unlike what was verified for compound **8a**, none of the possible binding modes of **8b** presented a binding free energy more favourable or comparable than the azaindole orientation of BMS.

3.10. Compound *8a* vs. *8b*

Only one binding mode was found for compound **8a** against three possible for **8b**. One of the orientations of the *R*-enantiomer was discarded as a possible binding mode based on the small

Table 5
H bonds formed between gp120 wt and binding modes of compounds **8a** and **8b**.

	Donor	Acceptor	Duration (% of the total simulation time considered)	Mean distance (Å)	Mean angle (°)
8a	C=O (α-ketoamide moiety)	H—N (Met475)	86	3.0	21
	C=O (carbamate moiety)	H—N (Gly431)	77	3.1	20
8b (cap)	N (azaindole moiety)	H—N (His105)	95	3.0	26
8c (phenyl)	C=O (carbamate moiety)	H_2N (Arg476)	99	2.9	23

Table 6
Decomposition of ($\Delta G_{gas+solv}$) on a pairwise-residue basis into apolar ($\Delta E_{vdw} + \Delta G_{(GB)np}$) and polar contributions ($\Delta E_{ele}\Delta G_{(GB)p}$), for the complexes of gp120 wt with the binding modes of compounds **8a** and **8b**. Values in bold represent significant interactions to the binding free energy.

Residue number[a]	**8a**			**8b**_cap			**8b**_azaindole			**8b**_phenyl		
	Apol[b]	Pol[c]	Total	Apol[b]	Pol[c]	Total	Apol	Pol	Tot	Apol	Pol	Total
His105	−0.7	0.0	−0.7	**−0.9**	**−1.9**	**−2.8**	0.0	0.0	0.0	−1.3	−0.9	−2.1
Ser256	−0.6	0.0	−0.6	−0.2	0.0	−0.2	−0.7	0.2	−0.5	−0.2	0.1	−0.1
Asp368	−1.0	0.2	−0.8	−1.5	0.1	−1.4	−1.5	−0.3	−1.8	−0.8	0.1	−0.7
Glu370	−0.2	0.0	−0.2	−1.5	0.0	−1.5	−2.0	0.1	−1.9	−1.1	0.3	−0.8
Ile371	−3.5	−0.2	−3.7	−2.3	0.0	−2.3	**−2.6**	**0.0**	**−2.6**	−1.0	0.0	−1.0
Asn425	**−4.1**	**−0.4**	**−4.5**	−0.5	−0.2	−0.7	**−3.7**	**−0.2**	**−3.9**	**−3.0**	**−0.7**	**−3.7**
Met426	**−2.2**	**−1.5**	**−3.7**	−0.9	−0.3	−1.2	−1.1	−1.2	−2.3	−1.9	0.2	−1.7
Trp427	**−3.0**	**−0.5**	**−3.5**	**−3.7**	**0.1**	**−3.6**	−2.0	−0.3	−2.3	**−3.3**	**0.2**	**−3.1**
Lys429	**−2.6**	**−0.7**	**−3.3**	**−3.1**	**−0.9**	**−4.0**	−0.6	−0.1	−0.7	**−3.0**	**−1.3**	**−4.3**
Val430	**−5.9**	**−0.8**	**−6.7**	**−2.8**	**−0.1**	**−3.0**	−2.2	−0.1	−2.3	**−4.5**	**−0.4**	**−4.9**
Gly431	−1.2	−0.6	−1.8	−0.1	0.0	−0.1	−0.5	0.0	−0.5	−0.4	0.1	−0.3
Gly473	−2.1	0.0	−2.1	**−4.6**	**−0.9**	**−5.5**	**−3.8**	**0.0**	**−3.8**	**−2.6**	**−0.5**	**−3.1**
Asp474	**−2.3**	**−0.3**	**−2.6**	**−3.4**	**−2.0**	**−5.3**	−2.3	0.1	−2.2	**−4.2**	**0.6**	**−3.6**
Met475	**−5.2**	**−1.4**	**−6.6**	−1.7	−0.1	−1.8	−0.7	0.1	−0.6	−1.0	0.0	−1.0
Arg476	−0.8	−0.3	−1.1	**−1.6**	**−1.3**	**−2.9**	0.0	0.0	0.0	**−2.8**	**−4.5**	**−7.3**
Total	−35.4	−6.5	−41.9	−28.8	−7.5	−36.3	−23.7	−1.7	−25.4	−30.7	−6.7	−37.7

All energies are in kcal mol^{-1}.
[a] The residue number is according to the HIV-1 gp160 sequence.
[b] Apol = $\Delta E_{vdw} + \Delta G_{(GB)np}$.
[c] Pol = $\Delta E_{ele} + \Delta G_{(GB)p}$.

binding free energy value, −25.7 kcal mol^{-1}, when compared to the other two. The orientation of compound **8b** that presents the higher binding affinity, cap binding mode, is now compared to its enantiomer, **8a**.

Both molecules bind to gp120 wt with similar binding modes, *i.e.*, with the phenyl situated at the entrance of the Phe43 cavity. Although the two molecules are enantiomers, the same moieties were found to occupy the same conformational space but with distinct orientation within it (Fig. 11A). In fact, the carbamate group is directed to the top of the entrance of the cavity, accommodating into a small groove and the azaindole ring is located just above the small arm of gp120. However, the stereochemistry of the carbon is more favourable to the binding of compound **8a** than compound **8b**. Indeed, the *S* configuration of the carbamate moiety allows the molecule to insert the phenyl moiety more deeply into the cavity and, consequently, a better fitting of the carbamate into the small groove (Fig. 11B). Also, the azaindole ring is placed parallel to the surface of the small arm of the protein favouring hydrophobic contacts. The better accommodation and binding observed for **8a** along with the values of binding free energy compared to **8b**, −44.7 and −34.0 kcal mol^{-1}, respectively, suggest that the enantiomers should present different binding affinities and that **8a** is susceptible to bind, to gp120 wt, more tightly than **8b**.

3.11. Conformational adaptability of compound *8a*

Our results pointed out compound **8a** as the enantiomer (*S*-enantiomer) that presents a better profile to bind to gp120 wt. Thus, we performed a conformational analysis for dihedral c and d of **8a** as we did for BMS. Fig. 12 shows the contours of potential energy for these torsional angles. The values of dihedral pair c–d are plotted in blue for **8a** free in solution and in orange for the binding orientation when complexed with HIV-1 gp120 wt.

From the plot, we observed that the conformational change that compound **8a** needs to undergo to bind to gp120 wt, demands an energy penalty of approximately 10 kcal mol^{-1}. This value is of the same order of magnitude than the value of the energy barrier required for the conformational change of the unbound BMS into the phenyl orientation. Also, we previously hypothesized that such energy barrier is "responsible" for the fact that phenyl orien-

Table 7
MM-PBSA interactions energies for the complexes of gp120 wt with the binding modes of compounds **8a** and **8b**. All values of energies are in kcal mol^{-1}.

Contribution	**8a**		**8b**_cap		**8b**_azaindole		**8b**_phenyl	
	Mean	STD	Mean	STD	Mean	STD	Mean	STD
ΔE_{ele}	−15.2	4.2	−27.1	5.2	−5.8	4.3	−17.1	4.7
ΔE_{vdw}	−53.4	3.2	−43.6	2.7	−36.8	3.6	−43.3	3.0
ΔE_{gas}	−68.6	5.9	−70.6	5.6	−42.6	4.0	−60.4	5.7
ΔG_{np} (solvation, non-polar)	−41.5	1.2	−37.2	1.5	−34.6	2.5	−33.7	1.3
ΔG_{p} (solvation, polar)	42.9	4.7	49.8	6.2	31.0	7.1	38.7	4.2
$\Delta E_{gas} + \Delta G_{solv}$	−67.2	4.0	−58.1	5.2	−46.2	5.7	−55.4	4.2
$-T\Delta S_{gas}$	22.5	7.9	24.1	9.8	20.5	8.4	23.5	8.0
ΔG_{bind}	−44.7	8.6	−34.0	11.1	−25.7	10.2	−31.9	9.0

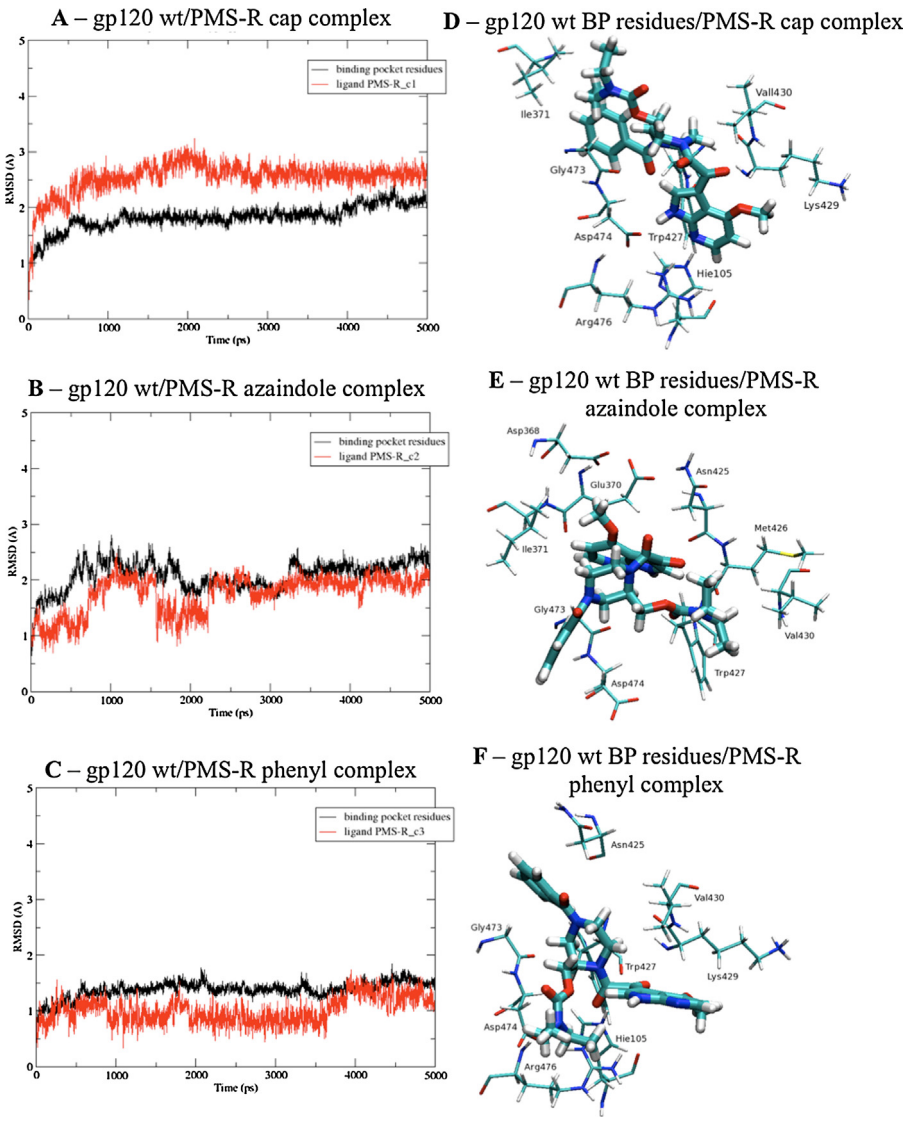

Fig. 10. Representation of the all-atom RMSD of the trajectory, of the gp120 wt residues within 5 Å from the ligand (black) and the ligand (in red), for the complexes with the cap (A), azaindole (B) and phenyl (C) binding modes of compound **8b**. The averages structure of each complex correspond to figures (D), (E) and (F), respectively. (For interpretation of the references to colour in this figure legend, the reader is referred to the web version of the article.)

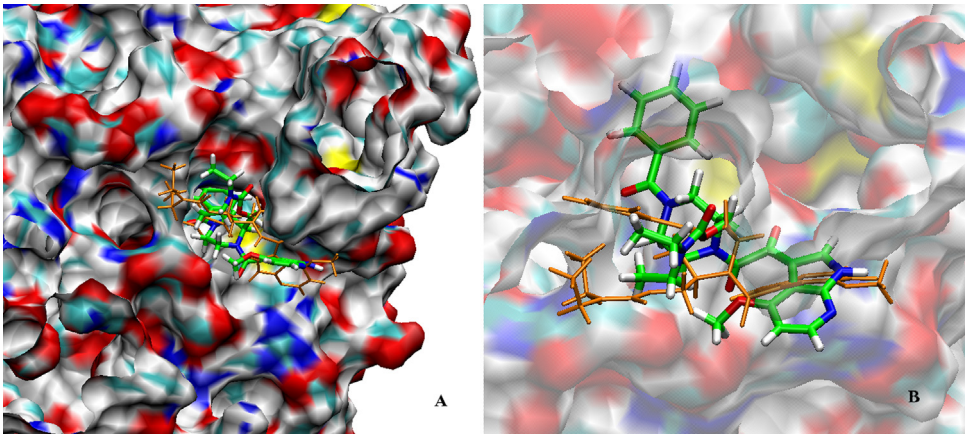

Fig. 11. (A) Representation of compound **8a** (in colours) and cap binding mode of compound **8b** (orange) complexed with gp120 wt (surface) (B) zoom-in of the Phe43 cavity, the surface of the protein is represented in transparent. (For interpretation of the references to colour in this figure legend, the reader is referred to the web version of the article.)

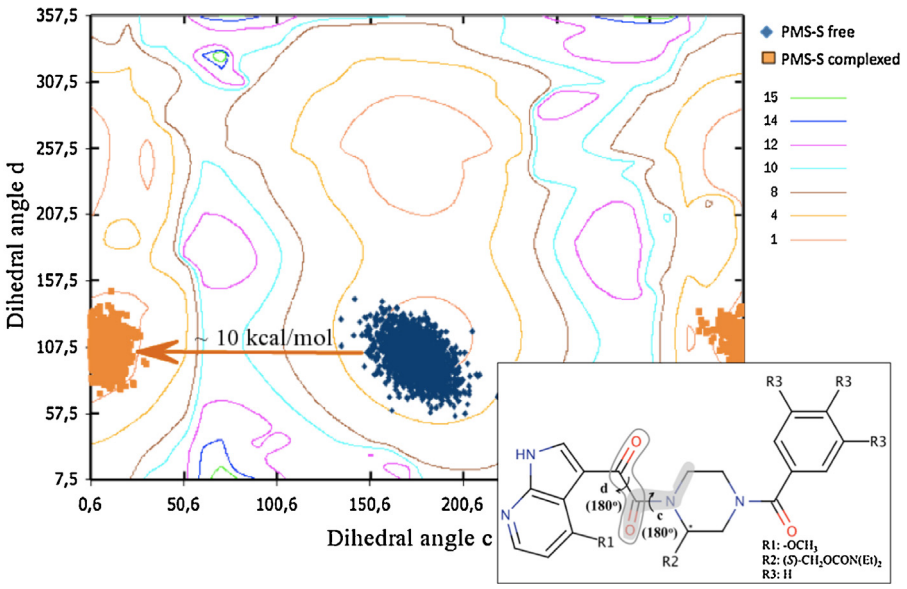

Fig. 12. Contours of potential energy for the dihedral pair c–d of compound **8a**. The values of the dihedrals angles c–d in the unbound and bound orientation are represented in blue and orange, respectively. The arrows show the conformational change that the free ligand needs to undergo to adopt the phenyl binding mode. (For interpretation of the references to colour in this figure legend, the reader is referred to the web version of the article.)

tation of BMS is unable to compete with CD4. Therefore, following the same reasoning and despite the good results for the predicted binding affinity of **8a** obtained from MD, it was also found that this molecule should undergo a significant conformational change to adopt the preferred conformation that binds to the protein. Thus, it is likely that this required conformational adaptability hinders compound **8a** to compete with CD4 binding as it was observed by experimental results (*cf.* Table 1). The inhibitory activity of the compounds against HIV-1 gp120 was evaluated in peripheral blood mononuclear cells culture infected *in vitro*. The results showed that both compounds **8a** and **8b**, unlike BMS, did not inhibit HIV-1 replication. It is noteworthy that the experimental results evaluated the capability of the piperazine derivatives in inhibiting the replication of the virus on cells that express CD4 receptor. Thus, they did not provide any information about the non-competitive binding of the molecules to HIV-1 gp120 but only on their ability to compete with CD4 binding. Concerning the competition with CD4, the experimental results for compound **8a** supported the hypothesis that a conformational change, between the unbound and bound orientations of the molecule, demanding a high-energy barrier hampers the compound to compete with CD4 gp120 binding. Hence, as for the phenyl conformation of BMS, it would be of great interest to modify the structure of compound **8a** in order to favour a conformation of the ligand free in solution close to its binding mode so they could act as competitive inhibitors with CD4 to HIV-1 gp120 binding.

4. Conclusion

We have presented an approach combining molecular docking, molecular dynamics and MM-PBSA calculations to rationally predict the binding mode of piperazine derivatives as potential inhibitors of HIV-1 gp120. As molecule of reference, we used BMS since previous studies demonstrated that this molecule inhibits the interaction between gp120 and CD4 and that this inhibition is the result of a specific compound binding to gp120. In order to validate our results for the predicted binding mode of BMS, we also performed the same molecular modelling procedure but using the mutant gp120 S375W, which is resistant to BMS. The results of the MD simulations with the mutant confirmed that the azaindole orientation is the binding mode responsible for the inhibitory activity of BMS towards HIV-1 gp120 wt. In fact, we observed that the azaindole binding mode was "kicked out" by the mutant and moved far way from the binding site. Regarding the MD analysis of compounds **8a** and **8b**, we observed that it is necessary to control the stereochemistry of the chiral carbon of the piperazine ring since it seems to have an impact on the binding free energy of these enantiomers with values of −44.7 and −34.0 kcal mol^{-1}, respectively.

Furthermore, we also inquired about the conformational adaptability of the molecules, upon complex formation, and its importance to their respective inhibitory activity. The conformational analysis (2D-grid search) for BMS combined with the results of molecular dynamics, showed that the azaindole binding mode is more accessible to protein binding than the phenyl one. The conformational energy cost for the ligand to adopt the geometry in the complex is only 2.0 kcal mol^{-1} for azaindole orientation and much higher for the phenyl, 10 kcal mol^{-1}. For **8a**, the conformational analysis exhibited an energy penalty of 10 kcal mol^{-1} to move from the free state to the bound conformation. Thus, despite the capability of these molecules to bind to the protein with distinct conformations due to their high degree of flexibility, only the conformationally available orientations will have the ability to compete with CD4 for HIV-1 gp120 binding. This was the case for compound **8a** that despite its predicted potential inhibitory activity, experimental results disclosed that this compound did not inhibit HIV-1 replication.

It is well known that molecular flexibility is a significant factor in biological activity. In the analysis of biological active factors, it is necessary to consider the flexible structural features of molecules. In one hand if one molecule is too flexible, it can adopt too many conformations and thus will likely have increased toxicity because it can bind to too many off target sites. On the other hand, if a molecule is too rigid, it might not be able to negotiate entry into the environment of the receptor site. So, in the analysis of molecular interaction between a ligand and its target, verification of the dynamic structural features of these molecules is indispensable. In this regard, our results clearly suggested that modifying the molecular structures of the piperazine derivatives, locking strategic dihedral angles (such as c and d) to the active conformation,

could improve the biological activity of the molecules. To our knowledge this is the first study concerning the impact of conformational adaptability for piperazine derivatives, which revealed to have a higher impact, in the context of drug design of HIV-1 gp120 inhibitors, than it has generally been assumed. These new insights at atomic level into the binding mode of piperazine derivatives and the importance of the flexibility of such molecules might be useful to design improved inhibitors.

Acknowledgements

We are grateful for the financial support from Fundação para a Ciência e a Tecnologia (Portugal) for the PhD fellowship SFRH/BD/22190/2005 to Cátia Teixeira. The authors thank the French National Agency for Research on AIDS and Viral Hepatitis (ANRS) for grant no. 07-341 (contrat d'initiation d'une recherche). Thank you to Pr. M. Malacria (Institut Parisien de Chimie Moléculaire, Université Pierre et Marie Curie, France) for technical NMR assistance. This work has benefited from the facilities and expertise of the Small Molecule Mass Spectrometry platform of IMAGIF (Centre de Recherche de Gif – www.imagif.cnrs.fr).

Appendix A. Supplementary data

Supplementary data associated with this article can be found, in the online version, at http://dx.doi.org/10.1016/j.jmgm.2013.05.003.

References

[1] C. Teixeira, J.R. Gomes, P. Gomes, F. Maurel, F. Barbault, European Journal of Medicinal Chemistry 46 (4) (2011) 979.
[2] H.G. Wang, R.E. Williams, P.F. Lin, Current Pharmaceutical Design 10 (15) (2004) 1785.
[3] P.F. Lin, W. Blair, T. Wang, T. Spicer, Q. Guo, N. Zhou, Y.F. Gong, H.G. Wang, R. Rose, G. Yamanaka, B. Robinson, C.B. Li, R. Fridell, C. Deminie, G. Demers, Z. Yang, L. Zadjura, N. Meanwell, R. Colonno, Proceedings of the National Academy of Sciences of the United States of America 100 (19) (2003) 11013.
[4] Z. Si, N. Madani, J.M. Cox, J.J. Chruma, J.C. Klein, A. Schon, N. Phan, L. Wang, A.C. Biorn, S. Cocklin, I. Chaiken, E. Freire, A.B. Smith 3rd, J.G. Sodroski, Proceedings of the National Academy of Sciences of the United States of America 101 (14) (2004) 5036.
[5] B. Chen, E.M. Vogan, H. Gong, J.J. Skehel, D.C. Wiley, S.C. Harrison, Nature 433 (7028) (2005) 834.
[6] H.T. Ho, L. Fan, B. Nowicka-Sans, B. McAuliffe, C.B. Li, G. Yamanaka, N. Zhou, H. Fang, I. Dicker, R. Dalterio, Y.F. Gong, T. Wang, Z. Yin, Y. Ueda, J. Matiskella, J. Kadow, P. Clapham, J. Robinson, R. Colonno, P.F. Lin, Journal of Virology 80 (8) (2006) 4017.
[7] N. Madani, A.L. Perdigoto, K. Srinivasan, J.M. Cox, J.J. Chruma, J. LaLonde, M. Head, A.B. Smith 3rd, J.G. Sodroski, Journal of Virology 78 (7) (2004) 3742.
[8] N. Serradji, O. Bensaid, M. Martin, E. Kan, N. Dereuddre-Bosquet, C. Redeuilh, J. Huet, F. Heymans, A. Lamouri, P. Clayette, C.Z. Dong, D. Dormont, J.J. Godfroid, Journal of Medicinal Chemistry 43 (11) (2000) 2149.
[9] D. Eggert, P.K. Dash, N. Serradji, C.Z. Dong, P. Clayette, F. Heymans, H. Dou, S. Gorantla, H.A. Gelbard, L. Poluektova, H.E. Gendelman, Journal of Neuroimmunology 213 (1/2) (2009) 47.
[10] R. Kong, J.J. Tan, X.H. Ma, W.Z. Chen, C.X. Wang, Biochimica et Biophysica Acta 1764 (4) (2006) 766.
[11] F. Barre-Sinoussi, J.C. Chermann, F. Rey, M.T. Nugeyre, S. Chamaret, J. Gruest, C. Dauguet, C. Axler-Blin, F. Vezinet-Brun, C. Rouzioux, W. Rozenbaum, L. Montagnier, Science 220 (4599) (1983) 868.
[12] A. Roisin, J.P. Robin, N. Dereuddre-Bosquet, A.L. Vitte, D. Dormont, P. Clayette, P. Jalinot, The Journal of Biological Chemistry 279 (10) (2004) 9208.
[13] G. Kärber, Naunyn-Schmiedebergs Archiv für Experimentelle Pathologie und Pharmakologie 162 (1931) 480.
[14] P.D. Kwong, R. Wyatt, S. Majeed, J. Robinson, R.W. Sweet, J. Sodroski, W.A. Hendrickson, Structure 8 (12) (2000) 1329.
[15] A. Barazarte, G. Lobo, N. Gamboa, J.R. Rodrigues, M.V. Capparelli, A. Alvarez-Larena, S.E. Lopez, J.E. Charris, European Journal of Medicinal Chemistry 44 (3) (2009) 1303.
[16] D.A. Case, T.A. Darden, T.E. Cheatham, C.L.I. Simmerling, J. Wang, R.E. Duke, R. Luo, M. Crowley, R.C. Walker, W. Zhang, K.M. Merz, B. Wang, S. Hayik, A. Roitberg, G. Seabra, K.F. Kolossváry, K.F. Wong, F. Paesani, F. Vanicek, X. Wu, S.R. Brozell, T. Steinbrecher, H. Gohlke, L. Yang, C. Tan, J. Mongan, V. Hornak, G. Cui, D.H. Mathews, M.G. Seetin, C. Sagui, V. Babin, Kollman PA, AMBER 9, University of California, San Francisco, 2006.
[17] L. Yang, C.H. Tan, M.J. Hsieh, J. Wang, Y. Duan, P. Cieplak, J. Caldwell, P.A. Kollman, R. Luo, The Journal of Physical Chemistry B 110 (26) (2006) 13166.
[18] A. Jakalian, B.L. Bush, D.B. Jack, C.I. Bayly, Journal of Computational Chemistry 21 (2) (2000) 132.
[19] J. Wang, R.M. Wolf, J.W. Caldwell, P.A. Kollman, D.A. Case, Journal of Computational Chemistry 25 (9) (2004) 1157.
[20] M.J.S. Dewar, D.M. Storch, Journal of the American Chemical Society 107 (13) (1985) 3898.
[21] T.I. Oprea, A.M. Davis, S.J. Teague, P.D. Leeson, Journal of Chemical Information and Computer Sciences 41 (5) (2001) 1308.
[22] Williams T., Kelley, C. Gnuplot 4.2: an interactive plotting program. URL http://www.gnuplot.info/docs_4.2/gnuplot.html (2007), (Last accessed: 2013 May 27).
[23] G.M. Morris, D.S. Goodsell, R.S. Halliday, R. Huey, W.E. Hart, R.K. Belew, A.J. Olson, Journal of Computational Chemistry 19 (14) (1998) 1639.
[24] C. Teixeira, N. Serradji, F. Maurel, F. Barbault, European Journal of Medicinal Chemistry 44 (9) (2009) 3524.
[25] W.L. Jorgensen, The Journal of Chemical Physics 77 (8) (1982) 4156.
[26] W.L. Jorgensen, J. Chandrasekhar, J.D. Madura, R.W. Impey, M.L. Klein, The Journal of Chemical Physics 79 (2) (1983) 926.
[27] T. Darden, D. York, L. Pedersen, The Journal of Chemical Physics 98 (12) (1993) 10089.
[28] S. Miyamoto, P.A. Kollman, Journal of Computational Chemistry 13 (8) (1992) 952.
[29] P.A. Kollman, I. Massova, C. Reyes, B. Kuhn, S. Huo, L. Chong, M. Lee, T. Lee, Y. Duan, W. Wang, O. Donini, P. Cieplak, J. Srinivasan, D.A. Case, T.E. Cheatham 3rd, Accounts of Chemical Research 33 (12) (2000) 889.
[30] N.A. Baker, D. Sept, S. Joseph, M.J. Holst, J.A. McCammon, Proceedings of the National Academy of Sciences of the United States of America 98 (18) (2001) 10037.
[31] D. Sitkoff, K.A. Sharp, B. Honig, Biophysical Chemistry 51 (2/3) (1994) 397.
[32] D. Sitkoff, K.A. Sharp, B. Honig, The Journal of Physical Chemistry 98 (7) (1994) 1978.
[33] J. Srinivasan, T.E. Cheatham, P. Cieplak, P.A. Kollman, D.A. Case, Journal of the American Chemical Society 120 (37) (1998) 9401.
[34] V. Zoete, M. Meuwly, M. Karplus, Proteins 61 (1) (2005) 79.
[35] H. Gohlke, C. Kiel, D.A. Case, Journal of Molecular Biology 330 (4) (2003) 891.
[36] R. Pauwels, J. Balzarini, M. Baba, R. Snoeck, D. Schols, P. Herdewijn, J. Desmyter, E. De Clercq, Journal of Virological Methods 20 (4) (1988) 309.
[37] J. Bostrom, P.O. Norrby, T. Liljefors, Journal of Computer-Aided Molecular Design 12 (4) (1998) 383.
[38] M.C. Nicklaus, S. Wang, J.S. Driscoll, G.W. Milne, Bioorganic & Medicinal Chemistry 3 (4) (1995) 411.
[39] K. Das, A.D. Clark Jr., P.J. Lewi, J. Heeres, M.R. De Jonge, L.M. Koymans, H.M. Vinkers, F. Daeyaert, D.W. Ludovici, M.J. Kukla, B. De Corte, R.W. Kavash, C.Y. Ho, H. Ye, M.A. Lichtenstein, K. Andries, R. Pauwels, M.P. De Bethune, P.L. Boyer, P. Clark, S.H. Hughes, P.A. Janssen, E. Arnold, Journal of Medicinal Chemistry 47 (10) (2004) 2550.